Article

Current Biology

Dynamic- and Frequency-Specific Regulation of Sleep Oscillations by Cortical Potassium Channels

Highlights

- A local screen shows different roles for potassium channels during sleep and wake
- Kv and KCa ion channels were locally important for cortical slow waves during sleep
- Depleting KCa1.1 reduces EEG power in sleep by slowing neuronal repolarization
- This reduction completely abolishes transcriptomic changes between sleep and wake

Authors

Christine M. Muheim, Andrea Spinnler, Tina Sartorius, ..., Clement Kabagema, Peter Ruth, Steven A. Brown

Correspondence

steven.brown@pharma.uzh.ch

In Brief

Muheim et al. convey two messages: first, that individual ion channels play roles specific to circadian and homeostatic brain "signatures" of sleep, and second, that the BK ion channel regulates both these signatures and their transcriptional consequences.

Muheim et al., 2019, Current Biology *29*, 1–10
September 23, 2019
https://doi.org/10.1016/j.cub.2019.07.056

CellPress

Please cite this article in press as: Muheim et al., Dynamic- and Frequency-Specific Regulation of Sleep Oscillations by Cortical Potassium Channels, Current Biology (2019), https://doi.org/10.1016/j.cub.2019.07.056

Current Biology
Article

Dynamic- and Frequency-Specific Regulation of Sleep Oscillations by Cortical Potassium Channels

Christine M. Muheim,[1,4] Andrea Spinnler,[1] Tina Sartorius,[2] Roland Dürr,[1] Reto Huber,[3] Clement Kabagema,[2] Peter Ruth,[2] and Steven A. Brown[1,5,*]

[1]Chronobiology and Sleep Research Group, Institute of Pharmacology and Toxicology, University of Zürich, Winterthurerstrasse 190, Zürich 8057, Switzerland

[2]Institute of Pharmacy, Department of Pharmacology, Toxicology and Clinical Pharmacy, University of Tübingen, Auf der Morgenstelle 8, Tübingen 72076, Germany

[3]University Children's Hospital Zurich, University of Zürich, Steinwiesstrasse 75, Zürich 8032, Switzerland

[4]Present address: Department of Biomedical Sciences, Elson S. Floyd College of Medicine, Washington State University, 412 E. Spokane Falls Boulevard, Spokane, WA 99202, USA

[5]Lead Contact

*Correspondence: steven.brown@pharma.uzh.ch

https://doi.org/10.1016/j.cub.2019.07.056

SUMMARY

Primary electroencephalographic (EEG) features of sleep arise in part from thalamocortical neural assemblies, and cortical potassium channels have long been thought to play a critical role. We have exploited the regionally dynamic nature of sleep EEG to develop a novel screening strategy and used it to conduct an adeno-associated virus (AAV)-mediated RNAi screen for cellular roles of 31 different voltage-gated potassium channels in modulating cortical EEG features across the circadian sleep-wake cycle. Surprisingly, a majority of channels modified only electroencephalographic frequency bands characteristic of sleep, sometimes diurnally or even in specific vigilance states. Confirming our screen for one channel, we show that depletion of the KCa1.1 (or "BK") channel reduces EEG power in slow-wave sleep by slowing neuronal repolarization. Strikingly, this reduction completely abolishes transcriptomic changes between sleep and wake. Thus, our data establish an unexpected connection between transcription and EEG power controlled by specific potassium channels. We postulate that additive dynamic roles of individual potassium channels could integrate different influences upon sleep and wake within single neurons.

INTRODUCTION

Beyond its evident behavioral manifestations, sleep is characterized by widespread synchronized electroencephalographic oscillations of defined frequency: theta (4–8 Hz) during rapid eye movement sleep (REM-S) and delta and "slow waves" (less than 4 Hz) during non-REM sleep (NREM-S) [1]. Slow-wave oscillations during NREM-S, comprised of the summed electrical potentials of the underlying brain cells, vary markedly in local fashion [2–4]. They are thought to arise primarily (but probably not exclusively) from communication across thalamus and neocortex [5]. Their amount and power are proportional to time and quality of waking experience, fostering hypotheses about their recuperative roles for synaptic homeostasis [6], brain metabolism [7–9], and cellular stress [10, 11]. Thus, although sleep itself is mostly a global phenomenon, it is widely accepted that sleep electroencephalogram (EEG) oscillations have local, use-dependent intensity [3, 12, 13]. Second, in addition time awake, the circadian clock also regulates sleep. Therefore, a widely cited theoretical framework for understanding sleep is the "two-process model" of sleep regulation by circadian and homeostatic factors [14].

Recently, a number of genetic screens have highlighted specific proteins playing a role in sleep duration [15–17]. Within these screens, potassium channels have emerged as key players in the global regulation of sleep duration. Voltage-dependent potassium currents—which, broadly speaking, modulate both neuronal resting state potential and repolarization and therefore both tendency to fire and firing rate—have long been thought to be critical to oscillatory behavior in general [18] and to slow-wave sleep in particular [19]. Recent modeling suggests that calcium-dependent hyperpolarization by potassium currents could be an important aspect of sleep regulation, and global knockout of some calcium-dependent potassium channels alters the total minutes of sleep [15].

A corresponding investigation of the proteins regulating local EEG manifestations of sleep in freely behaving animals remains lacking. Presumably, potassium channels would also play an important role in these local cortical EEG oscillations. However, with 40 different voltage-gated potassium channels in cortex alone, their specific local roles remain unexplored.

In this paper, we designed a screen to probe the local importance of voltage-gated potassium channels to sleep EEG oscillations across sleep stages and circadian time. By injecting adeno-associated viruses (AAVs) expressing RNAi short hairpin RNA (shRNA) targeting these channels, we were able to reduce issues of toxicity inherent in total and global depletion of some of these

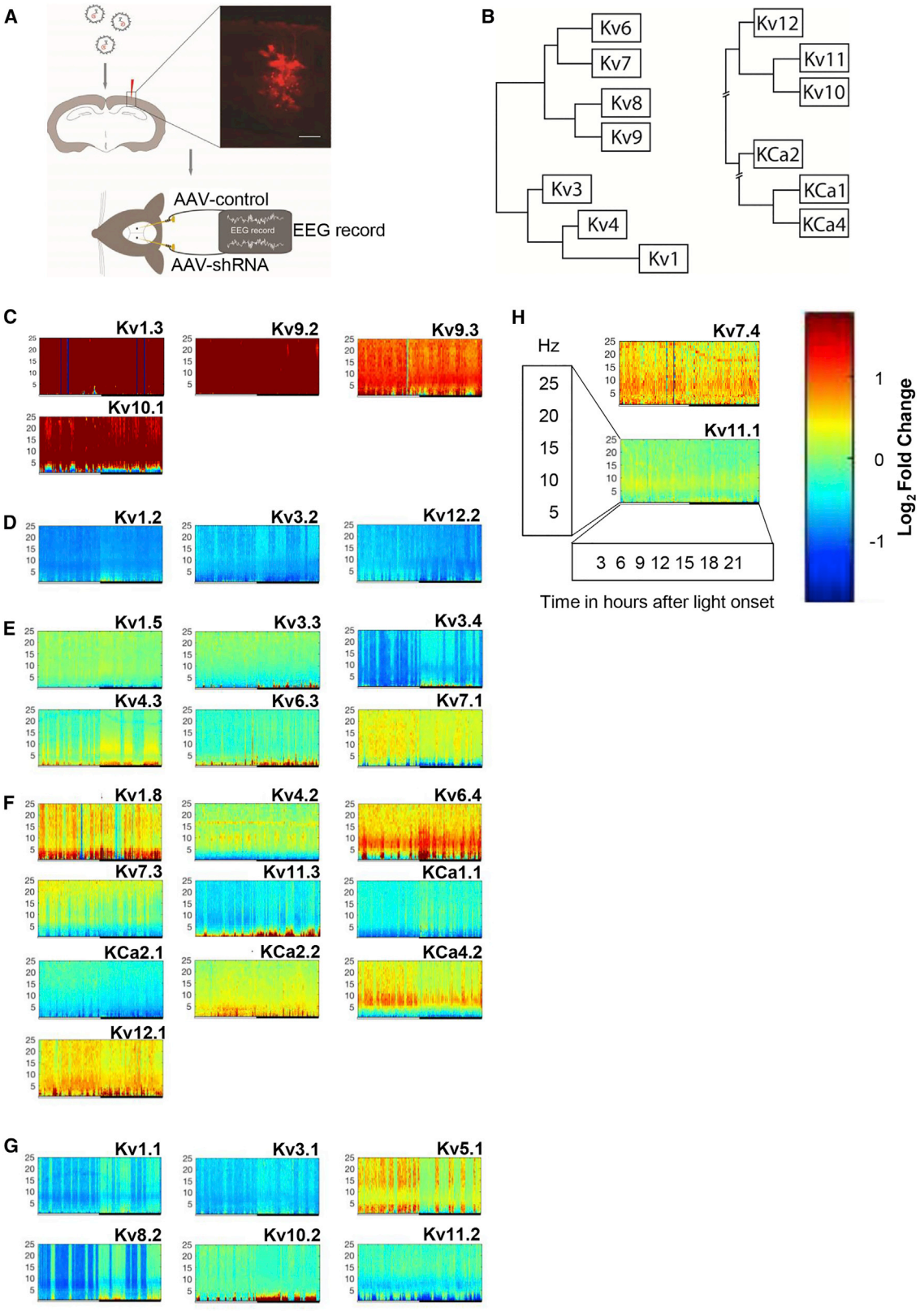

(legend on next page)

essential neuronal components and provide a broad look at their importance to spectral oscillations during sleep and wake. We find that members of this large class of channels exert unique nonredundant effects that vary with different stages of sleep and at different times of day. We further prove the cellular importance of these effects for a single channel by showing its importance for remodeling the cortical transcriptome in wake-dependent fashion.

RESULTS

An AAV-Mediated RNAi Screen for Cortical Ion Channels Important to Sleep EEG

For the current study, we developed an AAV that expressed an shRNA under control of the neuron-specific CAG promoter, as well as a tRFP fluorescent marker. Injection of shRNA-containing virus locally into one parietal cortex and injection of control virus expressing a scrambled hairpin into the same location contralaterally resulted in viral cassette expression locally within maximally 1 mm^3 of cortex (centered in layer IV) after several days. By placing a skull electrode directly above the injection site, we could then compare EEG frequencies on the two sides during wake and sleep (Figure 1A). Importantly, comparison of EEG power spectra for all vigilance states in opposite hemispheres using no or only control viruses showed no significant differences in spectral power (Figures S1A and S1B) and 92.5%–98.2% similarity in wake and NREM states (Figure S1C). By contrast, as a positive control, injection of virus overexpressing or reducing expression of *Adk2* [20]—encoding adenosine kinase and previously shown to regulate the intensity of NREM sleep [21]—increased or decreased local slow wave power as predicted from studies with global transgenic mice (Figure S1D). Therefore, we concluded that, at least in principle, local targeting of factors important to sleep could produce local differences in the intensity of slow waves that paralleled those observed in global transgenic mice.

Next, we developed AAV vectors containing RNAi hairpins targeting cortical potassium channels in two subfamilies, voltage-gated and calcium-gated, each validated *in vitro* by transfection into neuroblastoma N2 cells (Tables S1 and S2). From the 81 designed hairpins, 67 passed the quality control, targeting a total of 31 different potassium channels. These hairpins were used as the basis for an EEG screen for channels affecting local sleep, whose workflow is documented in Figure S1E. In brief, after hairpin design and validation *in vitro*, hairpins were unihemispherically injected into parietal cortex, along with control viral injection in the contralateral hemisphere (choice of experimental hemisphere was varied among mice of each group). EEG data were then plotted as a color map of the magnitude of changes in EEG spectral intensity in experimental hemisphere relative to control hemisphere for each channel and frequency bin over 24 h, with warm colors representing increases and cold colors decreases in the experimental hemisphere (Figures 1C–1H). As suggested by control experiments (Figures S1A and S1B), all the effects we report have resulted from changes in experimental and not control hemispheres; corresponding paired maps of absolute intensity for single representative mice can be found on Zenodo (https://doi.org/10.5281/zenodo.2653232, under supplementary item 1; single mice are depicted in order to match EEG power to the timing of sleep stages, unique to each mouse).

Overall, four groups of phenotypes could be identified: (1) channels that, when depleted, globally increased or decreased EEG power across all frequency bands (Figures 1C and 1D; such a result is consistent with a large literature about the role of potassium channels in regulation of neuronal oscillations) [22]; (2) channels that induced changes varying with respect to time of day or environmental light (Figure 1E), i.e., in which the left half of the relative power diagram is colored differently from the right half; (3) frequency-band-dependent effects (Figure 1F), where diagrams appeared vertically different (consistent with the cortical location of our depletions, these frequency-dependent effects were dominated by slow-wave-specific effects, because these frequencies are thought to arise primarily from a thalamocortical circuit) [23]; and (4) channels with changes of spectral power relative to vigilance state (Figure 1G), visible by the striped appearance of these relative diagrams. These phenotypic categories were not mutually exclusive, and many channels screened showed elements of one or more categories. Perhaps surprisingly, however, the smallest class was that with no major effects (Figure 1H).

The BK Channel Locally Regulates Cortical Sleep Slow-Wave Intensity

Supporting the validity of our experimental design, one class of channels that our screen identified as having effects upon oscillation is the Shaker family, shown previously to regulate sleep in both flies and mice [24, 25]. The related members of this family, like Kv1.1 or Kv1.2, had widespread effects across many oscillatory frequencies, but not specifically slow waves per se (Figures 2A and 2B).

Nevertheless, our screen also uncovered specific channel classes that preferentially regulate slow-wave oscillations, suggesting for the first time which channels might play roles in regulating regional NREM sleep depth. Among the most prominent in

Figure 1. State- and Frequency-Specific Changes in EEG Power after Depletion of Specific Ion Channels in Mouse Cortex

(A) Schematic drawing of the AAV2 injection site and localization of electrodes for EEG recordings on the mouse cortex. Inset, representative virally infected area expressing tRFP; scale bar, 200 μm.

(B) Dendrograms of cortical voltage-gated and calcium-activated potassium channel subfamilies screened.

(C–H) Relative EEG power (targeted versus control hemisphere power) for each channel over 24 h at baseline conditions plotted in 5-min bins, normalized per vigilance state. Per channel one representative animal is shown here to make sleep-stage-dependent changes apparent. Screen results can be grouped into 6 classes: generally upregulated (C), generally downregulated (D), circadian changes (E), spectral band-dependent changes (F), vigilance state dependent (G), or no effects (H). y axis, frequency in hertz; x axis, time in hours relative to light onset (black bar shows times of darkness); color scale, $\log_2$ fold-change of EEG power of experimental relative to control hemisphere.

See also Figures S1 and S2 and Tables S1 and S2.

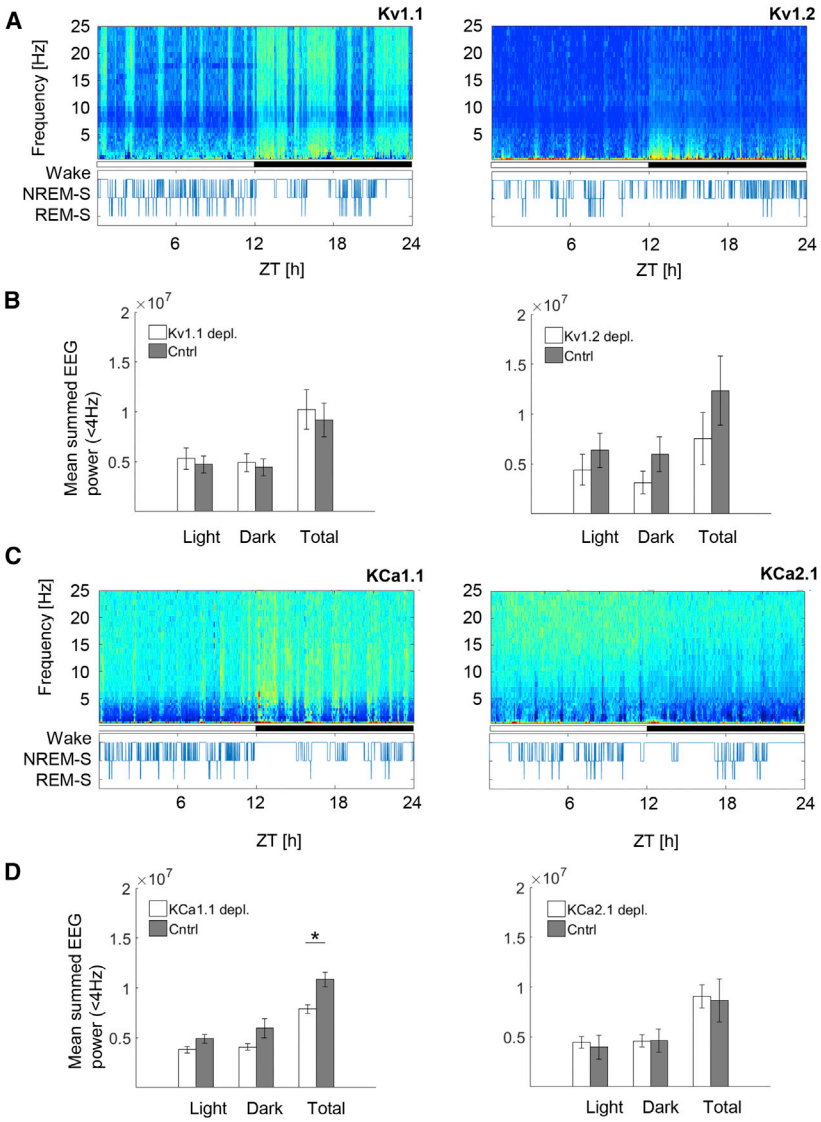

Figure 2. Local Depletion of 4 Ion Channels Indicates Family-Specific Functions

(A) Normalized fold changes of total spectral power for local knockdown of Kv1.1 and Kv1.2, plotted as log2 (spectral power at hairpin site relative to spectral power at control site) over 24 h. Data are plotted in 5-min bins for one representative animal, and the corresponding hypnogram is shown below. Relative EEG data are normalized per vigilance state. Color scale and axes are as in Figure 1.

(B) Summed absolute delta power in all states for 12 h light, 12 h dark, and 24 h total for Kv1.1 (left) and Kv1.2 (right). Open bars, hemisphere injected with small interfering RNA (siRNA) AAV; solid bars, control hemisphere.

(C) Same as (A) but depicting KCa1.1 and KCa2.1.

(D) Same as (B) but depicting KCa1.1 and KCa2.1. Plotted are means ± SEM; n = 3–6; ANOVA to test effects of the local ablation on total summed delta power; $F_{(1,30)} = 23.77$; significant for KCa1.1 with $p = 3.3 \times 10^{-5}$; *p = 0.0019; unpaired Student's t test. See also Figure S2.

this class were calcium-dependent potassium channels (KCa channels) KCa1.1 and KCa2.1. Suppression of those channels selectively reduced EEG power at lower frequencies more than at other frequency ranges independent of vigilance state and, in the case of KCa1.1, at all times of day (Figures 2C, 2D, 3A, and 3B). Importantly, EEG power of the local KCa1.1 knockdown showed no significant changes for other EEG spectral ranges.

The KCa1.1 channel—the voltage-gated, calcium-regulated, large-conductance potassium channel, or "Big K" channel, hereafter called "BK"—has been shown previously to regulate circadian spontaneous action potentials in the suprachiasmatic nuclei [26, 27], thereby increasing rodent activity during the daytime and decreasing activity at night. Moreover, mathematical modeling and global mouse knockout studies have suggested a role for BK in controlling total sleep time [15, 19]. To rule out the possibility that the effects we observed of BK depletion upon slow-wave frequencies were dependent upon changed circadian activity as reported previously in global and suprachiasmatic nuclei (SCN)-specific $BK^{-/-}$ mice [26, 28], we first verified that mouse activity and global sleep structure (minutes per unit time at different times of day) were unchanged (demonstrated already in Figure S1C and also true for all channels screened). This would be expected, because our injections were limited to a very small cortical region. Second, we examined slow wave power at six different times of day and demonstrated the same slow wave-specific reduction in power at all circadian times (Figure S2A). Finally, we demonstrated pharmacologically the same local EEG effects: we locally inhibited KCa1.1 channels using iberiotoxin injected at ZT2 in the same location as during the viral screen (Figure S2B) and could observe the same sleep-specific reduction in total EEG delta power following injection (Figure S2C). Thus, multiple independent lines of evidence support the hypothesis that KCa1.1 channels can regulate slow-wave EEG frequencies locally in the cortex, specifically during sleep and independently of the circadian clock.

$BK^{-/-}$ Mice Show Reduced Slow-Wave Power

We confirmed the idea that these EEG changes were KCa1.1 (i.e., BK)-driven by using a global mouse $BK^{-/-}$ knockout model [29]. As in the case of local RNAi-based or pharmacological depletion of BK activity, slow-wave power was reduced in both parietal and frontal derivations of $BK^{-/-}$ mice (Figure 3C). This phenotype was observed at all circadian times (Figure S3A). Consistent with the lower slow-wave power, NREM sleep episodes were also more fragmented (Figures S3B and S3C).

We next examined the effects of BK deficiency after a 4-h sleep deprivation by gentle handling at the time of light onset, when rodents would normally choose to sleep. A reduction in slow-wave power relative to control littermates was observed in both baseline conditions and after sleep deprivation (Figures 3C, 3D, and S3A). However, the increase in slow-wave power

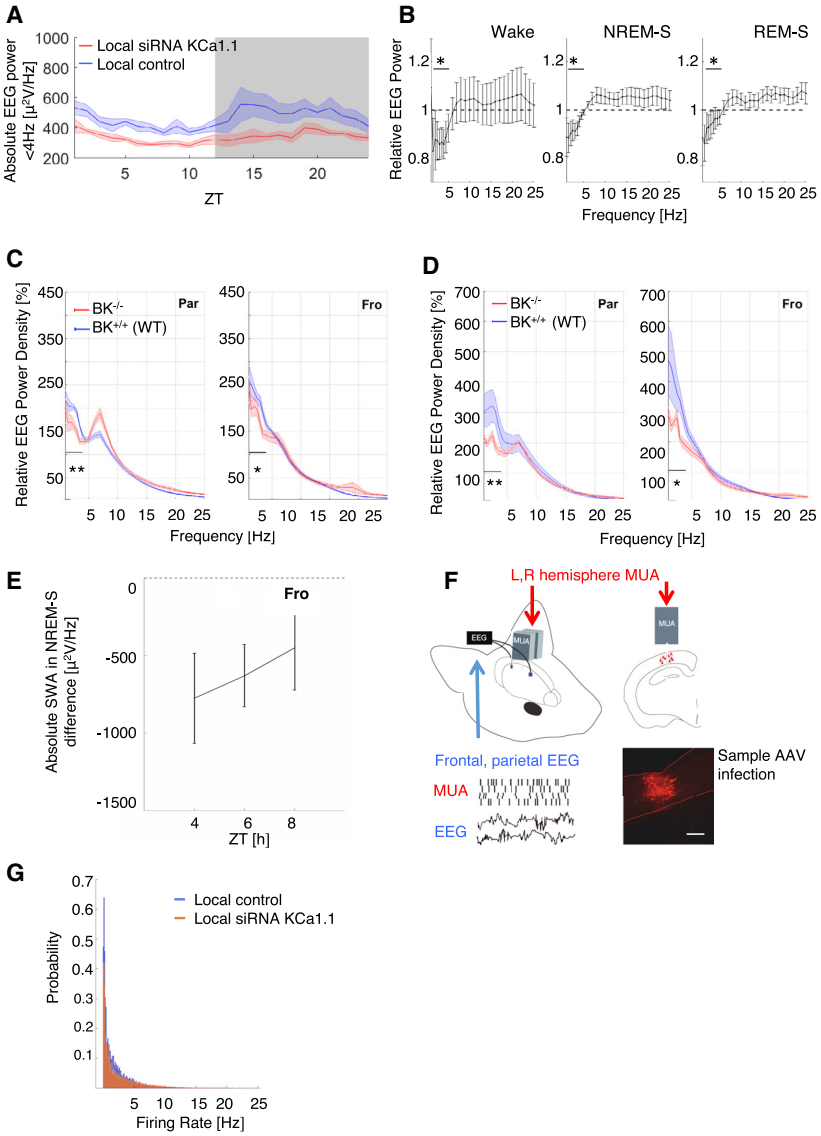

Figure 3. Disturbed Homeostatic Sleep in BK-Deficient Mice

(A) 24-h time course of absolute total delta power for local KCa1.1 knockdown; mean ± SEM (indicated by shading); n = 6.

(B) Relative spectrogram for local KCa1.1 knockdown (target relative to control), summed across the 12-h light period for each vigilance state (means ± SEM; n = 6; *p = 0.0154 [WAKE]; p = 9.02 × 10^{-6} [NREM-S]; p = 0.003 [REM-S]; unpaired Student's t test for delta; post hoc Bonferroni correction).

(C) Spectral power in parietal and frontal EEG derivations during NREM sleep under normal (baseline) conditions at ZT4–6 in $BK^{-/-}$ global knockout animals (red lines) and wild-type $BK^{+/+}$ controls, as a percentage of 24 h mean power, for frontal (Fro) and parietal (Par) EEG derivation. Line marks delta frequency range (<4 Hz); *p = 0.0039; **p = 0.0003.

(D) Identical to (C) but at ZT4–6 during recovery sleep after 4-h (ZT0–4) sleep deprivation; *p = 1.1 × 10^{-4}; **p = 7.7 × 10^{-7}; $BK^{-/-}$ n = 5; $BK^{+/+}$ n = 6.

(E) Decay in slow wave activity (SWA) in NREM sleep after 4 h sleep deprivation. Each time point is expressed as the difference $BK^{-/-}$ minus wild-type (WT) (2-h bins for each time point and animal; $BK^{-/-}$ n = 5; $BK^{+/+}$ n = 6; regression slope p = 0.008; t = −2.73).

(F) Schematic drawing of multiunit array and EEG electrode placement. Note: both LFP signals and single and multiunit waveforms were obtained from multi-electrode array (MEA) electrodes. The coronal section shows the local distribution of AAV infection, as visualized by its tRFP marker. Scale bar, 400 μm.

(G) Cumulative sum of normalized firing rate per 4-s epoch for the 2-h recording; n = 4 animals; Kruskal-Wallis test Chi^2 = 5.84; p = 0.0157; df = 1. Firing rate was normalized to the mean firing rate per animal.

See also Figures 4, S2, and S3.

that $BK^{-/-}$ mice experienced as a result of sleep deprivation was much less (Figures 3D and S4A). Second, during recovery NREM sleep after sleep deprivation, slow-wave power returned to baseline levels in both wild-type ($BK^{+/+}$) and $BK^{-/-}$ mice, but the two groups returned to baseline at different rates (Figure 3E). These results suggest specific dysregulation of homeostatic sleep—loosely speaking, a slowed accumulation and dissipation of "sleep pressure"—in BK-deficient mice.

Local Depletion of BK Channels in the Cortex Reduces Firing Frequency during Slow Waves

The exact circuit responsible for the generation of EEG slow waves remains controversial: although a widely accepted model from Steriade and colleagues suggests a thalamocortical circuit [30], nevertheless a cortical slab [31, 32] or even a plate of cultured neurons [33] can show slow-wave oscillatory activity. Common among these models, at a cellular level, EEG slow waves are reflective of synchronous underlying oscillations of bursting and quiescence in the neurons contributing to the EEG signal [34]. Therefore, to try to understand better the cellular effects of BK depletion, we examined the firing rate and spike profile across time of individual neurons during local RNAi depletion of BK (Figure 3F), implanting a single shank array with 16 electrodes per hemisphere in columnar fashion across the cortex. Importantly, in this experiment, local field potential (LFP) shows the same slow-wave-specific reduction in frequency observed in EEG in previous figures (Figure S4B). Next, examining the distribution of firing frequencies of individual computer-sorted "units" (presumably representing individual or highly similar neurons), we demonstrated that the overall firing rate is reduced (Figure 3G; Kruskal-Wallis; Chi^2 = 5.84; p = 0.0157; df = 1) and, consistent with this, that the interspike-interval distribution (ISI) was shifted rightward toward longer intervals (Figure S4C; p = 1.2 × 10−8; Wilcoxon rank test). Thus, one principal contributor to the reduction in slow-wave EEG upon BK depletion is the reduction in firing frequency during the "active" period of each EEG slow wave. At the same time, we could rule out the effects of synchrony among cells by aligning the spiking data with their relative electrode location in the cortex, comparing LFP and unit activity (Figures S4D and S4E). Thus, although defined cortical cell types

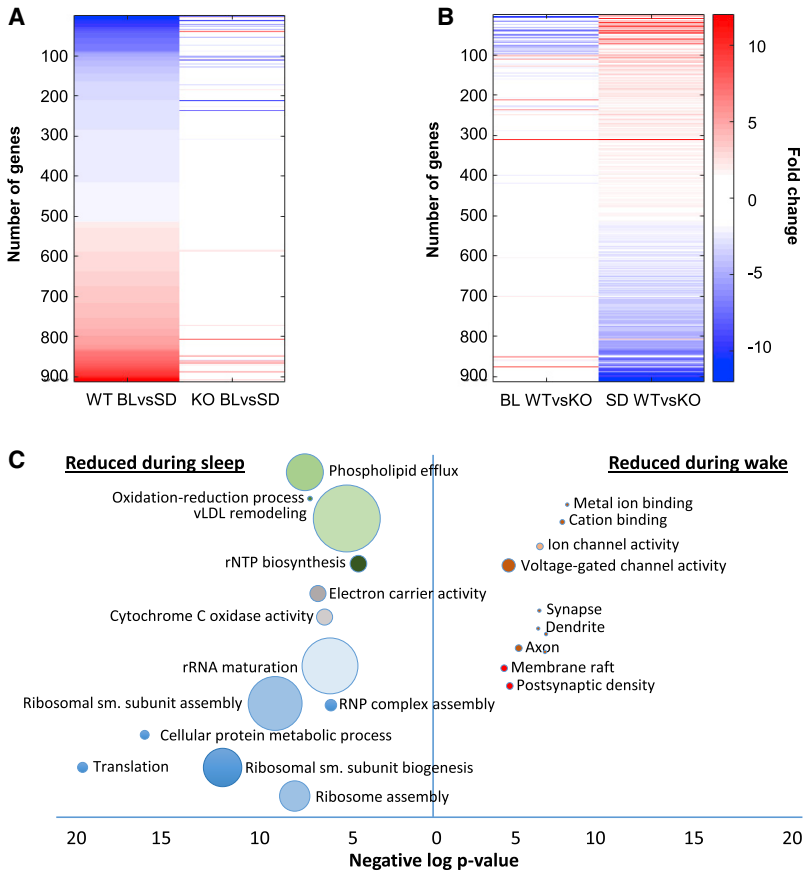

Figure 4. BK Activity Is Necessary for Sleep-Wake-Dependent Transcriptional Changes

(A) Heatmap of transcripts showing altered expression after 4 h sleep deprivation relative to baseline, either in $BK^{-/-}$ mice or their wild-type littermates (q = 0.05; fold change > 2).

(B) Heatmap of genes whose expression is altered in $BK^{-/-}$ mice compared to their wild-type littermates, either at baseline or after sleep deprivation (q = 0.05, fold change > 2).

(C) GO terms enriched for sleep versus sleep deprivation and WT/$BK^{-/-}$. Left: terms reduced during sleep are shown. Right: terms reduced during wake are shown. x axis, negative log p value for significance; circle size, percentage of genes affected in category. Similar categories are colored commonly; y axis is arbitrarily arranged for ease of reading. Data for this graph are listed in Data S1.

(D) Protein expression of two markers for inhibitory (GABA α 1) and excitatory (SynGap1) synapses at ZT4 after SD in a representative cortical staining is shown; 60× magnification; scale bar, 20 μm.

(E) Quantification of the relative cluster area (diameter of 0.1–1.5 μm^2) for GABAα1 staining. Student's t test; p = 0.0013; Bonferroni correction; n = 3 animals/genotype, 6–12 regions of interest (ROIs) per animal.

(F) Quantification for SynGAP1 staining for clusters between 0.1 and 4 μm^2; n = 3 animals/genotype, 3 ROIs per animal; Student's t test; p = 0.0071; Bonferroni correction.

See also Figure S4 and Data S2.

certainly contribute in specific ways to the slow-wave oscillation circuit (reviewed in [5, 23]), the fundamental effect of BK channel depletion upon EEG is likely a cell-autonomous one that slows firing rate, as has been demonstrated electrophysiologically in other studies [35–38].

BK Channel Ablation Suppresses Sleep/Wake-Dependent Transcriptomic Changes

Both in our local RNAi study and in the global BK knockout, total effects upon sleep and slow-wave power remain relatively modest. Therefore, we next set out to characterize the cellular consequences of BK depletion. Homeostatic sleep pressure has been defined not only classically by the accumulation and dissipation of slow waves [39] but also more recently by transcriptomic changes in cortical neurons, including effects upon immediate early genes, heat shock genes, and effectors of synaptic plasticity, like *Arc*, *Bdnf*, and *Homer1a* [10, 11, 40]. We performed deep sequencing of transcripts from cortex of wild-type and knockout mice under baseline conditions 4 h after light onset, during normal sleep (BL) (ZT4) or after 4 h of sleep deprivation (SD) during the same interval (ZT4).

Surprisingly, the transcriptional signature of sleep deprivation was not merely attenuated but virtually abolished: sleep deprivation results in dramatic transcriptomic changes in wild-type mice but virtually no changes in $BK^{-/-}$ mice (Figure 4A). Viewed another way, there are virtually no differences in the cortical transcriptome of $BK^{-/-}$ mice relative to wild-type under control conditions, but dramatic changes become visible as soon as the mouse is sleep deprived (Figure 4B).

We compared the set of genes showing changes in response to sleep deprivation and genotype (Data S1) and found a binary partition of these effects: terms entirely associated with synaptic components and activity were reduced during prolonged wake, and classes related to translation and cellular energy restoration were reduced during sleep (Figure 4C; listed in Data S1). Thus, the slow-wave impairment of BK mice translated roughly speaking into synapses that did not replenish cellular stores—or at least did not induce transcription of genes associated with these activities—during the sleep phase and did not induce synaptic changes as readily during the waking phase. The reduced synaptic components were evenly spread over

ontology terms associated with excitatory and inhibitory neurotransmission: collectively, we obtained Gene Ontology (GO): 0045202 synapse, false discovery rate (FDR) 5.44×10^{-5}, GO: 0045211 postsynaptic membrane, FDR 1.17×10^{-6}, GO: 0030425 dendrite, FDR 3.75×10^{-6}, GO: 0014069 postsynaptic density, FDR 4.6×10^{-4}, but when comparing alterations in expression of transcripts encoding proteins at inhibitory synapses versus excitatory ones [41–43], we found FDR = 0.9, suggesting that lack of BK function impacts upon both synaptic types.

These transcriptomic differences could be confirmed by immunohistochemistry. Staining for two postsynaptic marker genes—the inhibitory channel GABA-A α1 and SynGAP1, a highly abundant Ras GTPase regulating AMPA receptor trafficking [44]—we found reduced expression of both after sleep deprivation, localized in fewer synaptic speckles (Figures 4D–4F). Thus, BK channel activity is necessary to generate sufficient slow-wave amplitude during sleep and completely required to direct associated sleep-wake-dependent transcriptomic changes controlling synaptic composition.

DISCUSSION

In this paper, we exploited dynamic regional modulation of the sleep-wake EEG to develop an economical strategy for forward genetic screening and employed it to identify cortical potassium channels important to the regional EEG signature of sleep. Our novel screening method is adaptable to any class of molecule and uses local RNAi-based targeting to compare EEG signatures of sleep simultaneously in two cortical regions (one targeted and one control region). In this way, the local cortical contribution of a given molecule to EEG signatures of sleep can be isolated from possible global modulation by the same channels in other brain regions or from EEG changes arising from alterations in sleep structure (i.e., the minutes spent in any given sleep state).

In this study, we employ our novel screening method to look at cortical voltage- and calcium-gated potassium channels, by far the most complex and least-understood class of ion channels in the brain. A large number of voltage-dependent and voltage-and-calcium-dependent potassium channels are expressed in cortex, and inhibition or knockout of individual channels in mouse models have produced a wealth of brain phenotypes ranging from development [45] to epilepsy [46] to sleep [25, 47, 48], as well as renal [49], cardiac [50], and smooth muscle abnormalities [51]. Because these channels generally regulate neuronal excitability, they might play an important role in regulating synchronous oscillatory firing during sleep [22, 52]. *In vitro*, manipulating excitability regulates the propensity of neurons to enter into slow-wave oscillations [31, 33]. Supporting this idea, the principal outcome of multiple *Drosophila* reverse genetic screens for molecular components important to sleep has been voltage-gated potassium channels or their regulators (e.g., Sleepless and Shaker) [24, 53]. What has remained uncertain, however, is the degree of specificity that they might possess.

Surprisingly, we find that different channel subtypes contribute in frequency-, time-, and sleep-stage-specific fashion to EEG features of sleep at a local level. The majority of the channels that we screened affected EEG oscillations broadly across all frequencies, including channels with proven effects upon sleep like those of the Shaker family. However, a subset of channels affected particular frequency bands, vigilance states, or circadian times. Some of the "hits" in our screen are even thought to be electrically silent, such as the Kv6 and Kv10 families [54, 55]. Thus, on a general level, our screen suggests unsuspected complexity in the regulation of the activity of these channels. Such control could be imposed in a variety of ways, including channel expression, trafficking, post-translational modification, and control by other subunits.

As a model system to understand how channels uncovered in our screen might control the cellular physiology of sleep and wake, we focused upon one channel identified, the BK channel (KCa1.1 or KCNMA1), whose depletion affected primarily slow-wave frequencies in our experiments. Calcium-activated potassium current was predicted to be important to slow waves more than 20 years ago [19], and the BK channel has also been shown recently to modulate sleep duration by calcium-dependent hyperpolarization [15], as well as to control output from SCN neurons [28, 56, 57]. In this paper, we demonstrate that BK channels regionally control the intensity of slow-wave oscillations in freely moving animals. Electrophysiologically, this is not surprising: others have shown that this channel probably helps to repolarize neurons after action potentials, supporting the afterhyperpolarization phase by which inactivated voltage-dependent Na^+ and Ca^{2+} channels are reactivated [35]. Thus, it modulates interspike intervals [36] as we show and alters the propensity of individual neurons to enter into bistable oscillations [37, 38]. Globally, we show that BK depletion causes a change in the rate of recovery from sleep deprivation—i.e., changes in the rate of accumulation and dissipation of homeostatic sleep pressure within the two-process model for sleep regulation [39].

Depletion or deletion of BK channels resulted in moderate reductions specifically in regional slow-wave power. However, our transcriptomic dataset showed a much more dramatic result: almost total suppression of sleep-wake-dependent transcriptional changes in cortex. This suppression classed neatly into two categories: a reduction of metabolic changes during sleep and a reduction of synaptic changes during wake. These included components of both inhibitory and excitatory synapses, an effect that we could verify by immunohistochemistry. In an equilibrium situation across vigilance states, less firing in turn requires less inhibition, so BK channels might be important intermediaries in sleep-wake-dependent synaptic scaling. However, many aspects of this idea remain to be elucidated. For example, the specific neuronal circuitry that the BK channel modifies (i.e., the circuitry generating slow waves) remains unknown. We divided our detected units into putative pyramidal cells and interneurons by comparing firing peak widths and peak-to-trough ratios [58]. Effects were observed across all peak widths (Figures S4E–S4G), suggesting that BK loss affects firing of both types of neurons in the same cellular way; however, which specific neurons are necessary and sufficient for slow wave oscillations in the first place remains unaddressed. Moreover, recent work suggests that BK channels might also directly regulate gene expression via calcium signaling [52], suggesting another possible mechanism for transcriptomic modifications (NB: our transcriptomic results are derived from $BK^{-/-}$ mice, leaving open the further possibility that cortical transcriptome changes

could also be regulated indirectly by BK channels in other brain nuclei).

Overall, our screen shows a surprisingly complex and temporally specific influence of potassium channels on the cortical sleep EEG, as well as considerable cortical control of the sleep transcriptome by potassium channel subtypes controlling them. Because the effects of different channels upon membrane potential would be additive, such diversity would provide an ideal mechanism for a diversity of influences—environmental, circadian, and metabolic—to exert independent effects upon the sleep-wake cycle at a cellular level.

STAR★METHODS

Detailed methods are provided in the online version of this paper and include the following:

- KEY RESOURCES TABLE
- LEAD CONTACT AND MATERIALS AVAILABILITY
- EXPERIMENTAL MODEL AND SUBJECT DETAILS
- METHOD DETAILS
  - Surgeries
  - Data Acquisition and Analysis
  - Multi unit and LFP recordings
  - AAV vector design
  - AAV Production
  - RNA extraction and transcriptome analysis
  - Immunofluorescence
- QUANTIFICATION AND STATISTICAL ANALYSIS
- DATA AND CODE AVAILABILITY

SUPPLEMENTAL INFORMATION

Supplemental Information can be found online at https://doi.org/10.1016/j.cub.2019.07.056.

ACKNOWLEDGMENTS

C.M.M., R.H., and S.A.B. were supported by the Clinical Research Priority Program "Sleep and Health" of Zürich University Hospital and by the Swiss National Science Foundation. All are members of the Zürich Neurozentrum, a division of the Life Sciences Zürich graduate program. We thank Wolfger von der Behrens (University of Zurich) and Vlad Vyazovskiy (University of Oxford) for their advice with multi-unit activity recordings. Genomic services were provided by the Functional Genomics Center of the University of Zürich, with technical assistance from Catharine Aquino and bioinformatics assistance from Lennart Opitz and Weihong Qi. Equipment for sleep recording was constructed by Stefan Weber and Harald Osswald from the IPT Workshop, and assistance for optimization of sleep recordings was given by Harald Osswald. Additional thanks to J.M. Fritschy, C. Fraefel (University of Zürich), and D. Boison (Legacy Research, Portland) for kind donation of reagents and to Irene Tobler for critical reading of this manuscript and for procedural training.

AUTHOR CONTRIBUTIONS

Conceptualization, S.A.B. and C.M.M.; Methodology, S.A.B. and C.M.M.; Investigation, C.M.M., A.S., C.K., and T.S.; Data Curation, R.D. and C.M.M.; Writing – Original Draft, S.A.B. and C.M.M.; Visualization, C.M.M.; Funding Acquisition, S.A.B.; Resources, R.H. and P.R.; Supervision, S.A.B.

DECLARATION OF INTERESTS

The authors declare no competing interests.

Received: March 23, 2019
Revised: June 15, 2019
Accepted: July 17, 2019
Published: August 29, 2019

REFERENCES

1. Silber, M.H., Ancoli-Israel, S., Bonnet, M.H., Chokroverty, S., Grigg-Damberger, M.M., Hirshkowitz, M., Kapen, S., Keenan, S.A., Kryger, M.H., Penzel, T., et al. (2007). The visual scoring of sleep in adults. J. Clin. Sleep Med. *3*, 121–131.
2. Achermann, P., Finelli, L.A., and Borbély, A.A. (2001). Unihemispheric enhancement of delta power in human frontal sleep EEG by prolonged wakefulness. Brain Res. *913*, 220–223.
3. Huber, R., Ghilardi, M.F., Massimini, M., and Tononi, G. (2004). Local sleep and learning. Nature *430*, 78–81.
4. Vyazovskiy, V.V., Olcese, U., Hanlon, E.C., Nir, Y., Cirelli, C., and Tononi, G. (2011). Local sleep in awake rats. Nature *472*, 443–447.
5. Crunelli, V., and Hughes, S.W. (2010). The slow (<1 Hz) rhythm of non-REM sleep: a dialogue between three cardinal oscillators. Nat. Neurosci. *13*, 9–17.
6. Tononi, G., and Cirelli, C. (2003). Sleep and synaptic homeostasis: a hypothesis. Brain Res. Bull. *62*, 143–150.
7. Naidoo, N., Giang, W., Galante, R.J., and Pack, A.I. (2005). Sleep deprivation induces the unfolded protein response in mouse cerebral cortex. J. Neurochem. *92*, 1150–1157.
8. Porkka-Heiskanen, T. (1999). Adenosine in sleep and wakefulness. Ann. Med. *31*, 125–129.
9. Xie, L., Kang, H., Xu, Q., Chen, M.J., Liao, Y., Thiyagarajan, M., O'Donnell, J., Christensen, D.J., Nicholson, C., Iliff, J.J., et al. (2013). Sleep drives metabolite clearance from the adult brain. Science *342*, 373–377.
10. Maret, S., Dorsaz, S., Gurcel, L., Pradervand, S., Petit, B., Pfister, C., Hagenbuchle, O., O'Hara, B.F., Franken, P., and Tafti, M. (2007). Homer1a is a core brain molecular correlate of sleep loss. Proc. Natl. Acad. Sci. USA *104*, 20090–20095.
11. Terao, A., Wisor, J.P., Peyron, C., Apte-Deshpande, A., Wurts, S.W., Edgar, D.M., and Kilduff, T.S. (2006). Gene expression in the rat brain during sleep deprivation and recovery sleep: an Affymetrix GeneChip study. Neuroscience *137*, 593–605.
12. Huber, R., Ghilardi, M.F., Massimini, M., Ferrarelli, F., Riedner, B.A., Peterson, M.J., and Tononi, G. (2006). Arm immobilization causes cortical plastic changes and locally decreases sleep slow wave activity. Nat. Neurosci. *9*, 1169–1176.
13. Hung, C.-S., Sarasso, S., Ferrarelli, F., Riedner, B., Ghilardi, M.F., Cirelli, C., and Tononi, G. (2013). Local experience-dependent changes in the wake EEG after prolonged wakefulness. Sleep (Basel) *36*, 59–72.
14. Borbély, A.A. (1982). A two process model of sleep regulation. Hum. Neurobiol. *1*, 195–204.
15. Tatsuki, F., Sunagawa, G.A., Shi, S., Susaki, E.A., Yukinaga, H., Perrin, D., Sumiyama, K., Ukai-Tadenuma, M., Fujishima, H., Ohno, R., et al. (2016). Involvement of Ca(2+)-dependent hyperpolarization in sleep duration in mammals. Neuron *90*, 70–85.
16. Yoshida, K., Shi, S., Ukai-Tadenuma, M., Fujishima, H., Ohno, R.I., and Ueda, H.R. (2018). Leak potassium channels regulate sleep duration. Proc. Natl. Acad. Sci. USA *115*, E9459–E9468.
17. Funato, H., Miyoshi, C., Fujiyama, T., Kanda, T., Sato, M., Wang, Z., Ma, J., Nakane, S., Tomita, J., Ikkyu, A., et al. (2016). Forward-genetics analysis of sleep in randomly mutagenized mice. Nature *539*, 378–383.
18. Destexhe, A., Bal, T., McCormick, D.A., and Sejnowski, T.J. (1996). Ionic mechanisms underlying synchronized oscillations and propagating waves in a model of ferret thalamic slices. J. Neurophysiol. *76*, 2049–2070.
19. Metherate, R., and Ashe, J.H. (1993). Ionic flux contributions to neocortical slow waves and nucleus basalis-mediated activation: whole-cell recordings in vivo. J. Neurosci. *13*, 5312–5323.

20. Theofilas, P., Brar, S., Stewart, K.A., Shen, H.Y., Sandau, U.S., Poulsen, D., and Boison, D. (2011). Adenosine kinase as a target for therapeutic antisense strategies in epilepsy. Epilepsia *52*, 589–601.
21. Palchykova, S., Winsky-Sommerer, R., Shen, H.Y., Boison, D., Gerling, A., and Tobler, I. (2010). Manipulation of adenosine kinase affects sleep regulation in mice. J. Neurosci. *30*, 13157–13165.
22. Zagha, E., and McCormick, D.A. (2014). Neural control of brain state. Curr. Opin. Neurobiol. *29*, 178–186.
23. Steriade, M., Contreras, D., Curró Dossi, R., and Nuñez, A. (1993). The slow (< 1 Hz) oscillation in reticular thalamic and thalamocortical neurons: scenario of sleep rhythm generation in interacting thalamic and neocortical networks. J. Neurosci. *13*, 3284–3299.
24. Cirelli, C., Bushey, D., Hill, S., Huber, R., Kreber, R., Ganetzky, B., and Tononi, G. (2005). Reduced sleep in Drosophila Shaker mutants. Nature *434*, 1087–1092.
25. Douglas, C.L., Vyazovskiy, V., Southard, T., Chiu, S.Y., Messing, A., Tononi, G., and Cirelli, C. (2007). Sleep in Kcna2 knockout mice. BMC Biol. *5*, 42.
26. Meredith, A.L., Wiler, S.W., Miller, B.H., Takahashi, J.S., Fodor, A.A., Ruby, N.F., and Aldrich, R.W. (2006). BK calcium-activated potassium channels regulate circadian behavioral rhythms and pacemaker output. Nat. Neurosci. *9*, 1041–1049.
27. Whitt, J.P., Montgomery, J.R., and Meredith, A.L. (2016). BK channel inactivation gates daytime excitability in the circadian clock. Nat. Commun. *7*, 10837.
28. Kent, J., and Meredith, A.L. (2008). BK channels regulate spontaneous action potential rhythmicity in the suprachiasmatic nucleus. PLoS ONE *3*, e3884.
29. Sausbier, M., Hu, H., Arntz, C., Feil, S., Kamm, S., Adelsberger, H., Sausbier, U., Sailer, C.A., Feil, R., Hofmann, F., et al. (2004). Cerebellar ataxia and Purkinje cell dysfunction caused by Ca2+-activated K+ channel deficiency. Proc. Natl. Acad. Sci. USA *101*, 9474–9478.
30. Llinás, R.R., and Steriade, M. (2006). Bursting of thalamic neurons and states of vigilance. J. Neurophysiol. *95*, 3297–3308.
31. Sanchez-Vives, M.V., and McCormick, D.A. (2000). Cellular and network mechanisms of rhythmic recurrent activity in neocortex. Nat. Neurosci. *3*, 1027–1034.
32. Case, L., and Broberger, C. (2013). A method for visually guided whole-cell recordings in brain slices exhibiting spontaneous rhythmic activity. J. Neurosci. Methods *212*, 64–71.
33. Hinard, V., Mikhail, C., Pradervand, S., Curie, T., Houtkooper, R.H., Auwerx, J., Franken, P., and Tafti, M. (2012). Key electrophysiological, molecular, and metabolic signatures of sleep and wakefulness revealed in primary cortical cultures. J. Neurosci. *32*, 12506–12517.
34. Vyazovskiy, V.V., Olcese, U., Lazimy, Y.M., Faraguna, U., Esser, S.K., Williams, J.C., Cirelli, C., and Tononi, G. (2009). Cortical firing and sleep homeostasis. Neuron *63*, 865–878.
35. Jan, L.Y., and Jan, Y.N. (1990). How might the diversity of potassium channels be generated? Trends Neurosci. *13*, 415–419.
36. Gu, N., Vervaeke, K., and Storm, J.F. (2007). BK potassium channels facilitate high-frequency firing and cause early spike frequency adaptation in rat CA1 hippocampal pyramidal cells. J. Physiol. *580*, 859–882.
37. Pigorini, A., Sarasso, S., Proserpio, P., Szymanski, C., Arnulfo, G., Casarotto, S., Fecchio, M., Rosanova, M., Mariotti, M., Lo Russo, G., et al. (2015). Bistability breaks-off deterministic responses to intracortical stimulation during non-REM sleep. Neuroimage *112*, 105–113.
38. Rothberg, B.S. (2012). The BK channel: a vital link between cellular calcium and electrical signaling. Protein Cell *3*, 883–892.
39. Achermann, P., and Borbély, A.A. (1987). Dynamics of EEG slow wave activity during physiological sleep and after administration of benzodiazepine hypnotics. Hum. Neurobiol. *6*, 203–210.
40. Cirelli, C., Gutierrez, C.M., and Tononi, G. (2004). Extensive and divergent effects of sleep and wakefulness on brain gene expression. Neuron *41*, 35–43.
41. Fernández, E., Collins, M.O., Uren, R.T., Kopanitsa, M.V., Komiyama, N.H., Croning, M.D., Zografos, L., Armstrong, J.D., Choudhary, J.S., and Grant, S.G. (2009). Targeted tandem affinity purification of PSD-95 recovers core postsynaptic complexes and schizophrenia susceptibility proteins. Mol. Syst. Biol. *5*, 269.
42. Loh, K.H., Stawski, P.S., Draycott, A.S., Udeshi, N.D., Lehrman, E.K., Wilton, D.K., Svinkina, T., Deerinck, T.J., Ellisman, M.H., Stevens, B., et al. (2016).). Proteomic analysis of unbounded cellular compartments: synaptic clefts. Cell *166*, 1295–1307.e21.
43. Nakamura, Y., Morrow, D.H., Modgil, A., Huyghe, D., Deeb, T.Z., Lumb, M.J., Davies, P.A., and Moss, S.J. (2016). Proteomic characterization of inhibitory synapses using a novel pHluorin-tagged γ-aminobutyric acid receptor, type A (GABAA), α2 subunit knock-in mouse. J. Biol. Chem. *291*, 12394–12407.
44. Chen, H.J., Rojas-Soto, M., Oguni, A., and Kennedy, M.B. (1998). A synaptic Ras-GTPase activating protein (p135 SynGAP) inhibited by CaM kinase II. Neuron *20*, 895–904.
45. Duque, A., Gazula, V.R., and Kaczmarek, L.K. (2013). Expression of Kv1.3 potassium channels regulates density of cortical interneurons. Dev. Neurobiol. *73*, 841–855.
46. Robbins, C.A., and Tempel, B.L. (2012). Kv1.1 and Kv1.2: similar channels, different seizure models. Epilepsia *53* (*Suppl 1*), 134–141.
47. Espinosa, F., Torres-Vega, M.A., Marks, G.A., and Joho, R.H. (2008). Ablation of Kv3.1 and Kv3.3 potassium channels disrupts thalamocortical oscillations in vitro and in vivo. J. Neurosci. *28*, 5570–5581.
48. Vyazovskiy, V.V., Deboer, T., Rudy, B., Lau, D., Borbély, A.A., and Tobler, I. (2002). Sleep EEG in mice that are deficient in the potassium channel subunit K.v.3.2. Brain Res. *947*, 204–211.
49. Wen, D., Cornelius, R.J., and Sansom, S.C. (2014). Interacting influence of diuretics and diet on BK channel-regulated K homeostasis. Curr. Opin. Pharmacol. *15*, 28–32.
50. Frankenreiter, S., Bednarczyk, P., Kniess, A., Bork, N.I., Straubinger, J., Koprowski, P., Wrzosek, A., Mohr, E., Logan, A., Murphy, M.P., et al. (2017). cGMP-elevating compounds and ischemic conditioning provide cardioprotection against ischemia and reperfusion injury via cardiomyocyte-specific BK channels. Circulation *136*, 2337–2355.
51. Holtzclaw, J.D., Grimm, P.R., and Sansom, S.C. (2011). Role of BK channels in hypertension and potassium secretion. Curr. Opin. Nephrol. Hypertens. *20*, 512–517.
52. Li, B., Jie, W., Huang, L., Wei, P., Li, S., Luo, Z., Friedman, A.K., Meredith, A.L., Han, M.-H., Zhu, X.-H., and Gao, T.M. (2014). Nuclear BK channels regulate gene expression via the control of nuclear calcium signaling. Nat. Neurosci. *17*, 1055–1063.
53. Koh, K., Joiner, W.J., Wu, M.N., Yue, Z., Smith, C.J., and Sehgal, A. (2008). Identification of SLEEPLESS, a sleep-promoting factor. Science *321*, 372–376.
54. Ottschytsch, N., Raes, A.L., Timmermans, J.P., and Snyders, D.J. (2005). Domain analysis of Kv6.3, an electrically silent channel. J. Physiol. *568*, 737–747.
55. Vega-Saenz de Miera, E.C. (2004). Modification of Kv2.1 K+ currents by the silent Kv10 subunits. Brain Res. Mol. Brain Res. *123*, 91–103.
56. Belle, M.D.C., Diekman, C.O., Forger, D.B., and Piggins, H.D. (2009). Daily electrical silencing in the mammalian circadian clock. Science *326*, 281–284.
57. Pitts, G.R., Ohta, H., and McMahon, D.G. (2006). Daily rhythmicity of large-conductance Ca2+ -activated K+ currents in suprachiasmatic nucleus neurons. Brain Res. *1071*, 54–62.
58. Niell, C.M., and Stryker, M.P. (2008). Highly selective receptive fields in mouse visual cortex. J. Neurosci. *28*, 7520–7536.

59. Peixoto, L., Risso, D., Poplawski, S.G., Wimmer, M.E., Speed, T.P., Wood, M.A., and Abel, T. (2015). How data analysis affects power, reproducibility and biological insight of RNA-seq studies in complex datasets. Nucleic Acids Res. *43*, 7664–7674.

60. Deboer, T., Franken, P., and Tobler, I. (1994). Sleep and cortical temperature in the Djungarian hamster under baseline conditions and after sleep deprivation. J. Comp. Physiol. A Neuroethol. Sens. Neural Behav. Physiol. *174*, 145–155.

61. Franken, P., Dijk, D.J., Tobler, I., and Borbély, A.A. (1994). High-frequency components of the rat electrocorticogram are modulated by the vigilance states. Neurosci. Lett. *167*, 89–92.

62. Steck, A.J., and Perruisseau, G. (1980). Characterization of membrane markers of isolated oligodendrocytes and clonal lines of the nervous system. J. Neurol. Sci. *47*, 135–144.

63. Notter, T., Panzanelli, P., Pfister, S., Mircsof, D., and Fritschy, J.-M. (2014). A protocol for concurrent high-quality immunohistochemical and biochemical analyses in adult mouse central nervous system. Eur. J. Neurosci. *39*, 165–175.

64. Tyagarajan, S.K., Ghosh, H., Yévenes, G.E., Nikonenko, I., Ebeling, C., Schwerdel, C., Sidler, C., Zeilhofer, H.U., Gerrits, B., Muller, D., and Fritschy, J.M. (2011). Regulation of GABAergic synapse formation and plasticity by GSK3beta-dependent phosphorylation of gephyrin. Proc. Natl. Acad. Sci. USA *108*, 379–384.

STAR★METHODS

KEY RESOURCES TABLE

REAGENT or RESOURCE	SOURCE	IDENTIFIER
Antibodies		
Guinea Pig polyclonal anti-GABA-A α1	Laboratory of J-M Fritschy, UZH	N/A
Rabbit polyclonal anti-SynGap1	ThermoFisher	RRID: PA1-046
Bacterial and Virus Strains		
NEB 10-beta Competend E.coli	New England Biolabs	C3019I
AVV2-shRNA-tRPF (see Table S1)	This paper	N/A
Chemicals, Peptides, and Recombinant Proteins		
Iberiotoxin	ANAWA	PB0147 Batch 0147PB/10
Critical Commercial Assays		
ViraBind AAV Purification Kit	CellBiolabs	VPK140
Deposited Data		
EEG traces screen, raw and scored data	This paper	https://doi.org/10.5281/zenodo.2653232
RNaseq data, raw data set1	This paper	GEO: GSE132075
RNaseq data, raw data set2	This paper	GEO: GSE130276
Experimental Models: Cell Lines		
HEK293T	ATCC	ATCC: CRL-3216; RRID: CVCL_0063
Neuroblastoma 2A	ATCC	ATCC: CCL-131; RRID: CVCL_0470
Experimental Models: Organisms/Strains		
Mus musculus: C57Bl6/j	Jackson Laboratories	000664
Mus musculus: BK-SV129/C57BL6	[29]	N/A
Oligonucleotides		
shRNA oligos (see Table S1)	This paper	N/A
Oligo targets (see Table S1)	This paper	N/A
Recombinant DNA		
Plasmid: pCMV-luc	Laboratory of Steven A. Brown, UZH	N/A
Plasmid: pAVV2-shRNA-tRPF	This paper	N/A
Plasmid: pDG	Laboratory of Cornel Fraefel, UZH	N/A
Software and Algorithms		
MATLAB	MathWorks	R2018b
ImageJ	ImageJ	1.48J
Plexon Offline Sorter	Plexon	V4.3.1
NeuroExplorer	Neuroexplorer	https://www.neuroexplorer.com/
MultiChannel Suit (Data Acquisition and Analysis Software)	MultiChannelSystems	V4.6.2
edgeR (Version 3.8.2),	BioConductor	http://bioconductor.org/packages/release/bioc/html/edgeR.html
RUVseq	[59]	https://bioconductor.org/packages/release/bioc/html/RUVSeq.html

LEAD CONTACT AND MATERIALS AVAILABILITY

Further information and requests for resources and reagents should be directed to and will be fulfilled by the lead contact, Steven A. Brown (steven.brown@pharma.uzh.ch). Plasmids and AAVs generated in this study are available from the lead contact.

EXPERIMENTAL MODEL AND SUBJECT DETAILS

All experiments were conducted with the approval of relevant veterinary authorities in Switzerland and Germany. BK channel α-subunit-deficient mice ($BK^{-/-}$) were generated and maintained as described [29]. Litter-matched WT and $BK^{-/-}$ mice of male gender

with hybrid SV129/C57BL6 background (always F2 generation) were used. Mice were housed in a standard 12:12 L:D cycle, in normal cages prior to surgery, and then in open-top cages with counterbalanced swivel-attached cables during and between sleep recordings. Animals used for RNaseq experiments were 20 ± 2.7 (WT, n = 8) and 21.3 ± 3.2 ($BK^{-/-}$, n = 8) weeks old at the time of harvesting.

METHOD DETAILS

Surgeries

In general, methods used here mirror those in [21]. Cortical injections for the AAV screen were conducted with C57Bl6 mice, 3-4 months of age. The sleep phenotyping for the BK mutants were at the time of surgery 29.2 ± 10.5 weeks (littermate WT mice (n = 6)) and 20 ± 14.8 ($BK^{-/-}$ mice (n = 5)) weeks old. For the multiunit recordings 6 adult C57Bl6 mice were implanted bilaterally with a 16- channel 1-shank silicon probe (NeuroNexus, A1x16-3mm-100-177) 2mm anterior of lambda, +/− 1.5mm lateral to midline, with a depth of 1.5mm. A reference electrode was placed over the cerebellum, an additional ground electrode was place in the frontal lobe. The animal was given 2ug/gr Dexamethansone (s.c) over 27h starting 24h post-surgery. To prevent local inflammation, 100mg/kg. Ceftriaxone were administered i.v. during surgery along with the appropriate analgesia. To prevent systemic inflammation, the animals was given 100mg/ml Enrofloxacin (Baytril) over 7 days in the drinking water. For all sleep recordings mice were kept in Macrolon cages (36x20x35cm) with food and water *ad libitum* and maintained in a 12h light-dark cycle (light onset 07.00 AM). For the EEG recordings, mice were implanted epidurally with gold-plated miniature screws (0.9mm diameter) under constant isoflurane inhalation anesthesia. Analgesia was given i.p. at 0.1mg/kg. during the surgery. The screws were placed in the right frontal (1.5mm anterior to bregma, 2mm lateral to the midline) and right parietal hemisphere (2mm posterior to bregma and 3mm lateral of the midline). For the local depletion experiments both deviations were placed in the parietal cortex (2mm posterior to bregma and 3mm lateral of the midline) on both hemispheres. The reference was placed over the cerebellum (2mm posterior to lambda on the midline). Two gold wires (0.2mm diameter) were inserted bilaterally in the neck muscle for EMG recordings. The screws were connected to stainless steel wires and fixed on the skull with acrylic dental cement. All animals were tethered to a swivel throughout the experiment. Where appropriate, prior to electrode implantation 400-600nl of purified AAV (see below) dissolved in phosphate buffered saline (PBS, pH7.4) was infused at a rate of 50-200nl/min. Virus containing functional RNAi hairpin was infused on one side, and control virus on the other. The animals were allowed to recover for 4 to 7 days before any further handling.

Data Acquisition and Analysis

Sleep recordings were conducted in 24-hour periods under standard light:dark conditions. Sleep deprivation experiments were conducted for 4h starting at light onset (i.e., ZT0-4), using gentle handling [60] to keep animals awake without stress. The EEG and EMG signals for the local depletion experiments were amplified (amplification factor, ~2000), filtered (high pass filter: –3 dB at 0.016 Hz; low pass filter: –3 dB at 40 Hz) sampled with 512 Hz, digitally filtered [EEG: low pass finite impulse response (FIR) filter, 25 Hz; EMG: bandpass FIR filter, 20–50 Hz or 10-30Hz], and stored with a resolution of 128 Hz. The EEG power spectra were computed for 4 s epochs by a Fast Fourier transform routine. Adjacent 0.25 Hz bins were averaged into 0.5 Hz (0.25–5 Hz) and 1.0 Hz (5.25–25 Hz) bins. Before each recording, the EEG and EMG channels were calibrated with a 10 Hz, 300 μV peak-to-peak sine wave. Vigilance states (NREM, REM and wake) were visually determined, as previously documented by offline visual inspection of the EEG and EMG signals. Epochs containing artifacts in one derivation were excluded from spectral analysis of both EEG derivations. Vigilance state determination for the screen was done on a semiautomated basis using SleepSign (Kissey Comtech). The initial 2h of the baseline recording were taken to set up a logic file. For each animal, the logic file was adjusted individually and kept constant for the whole scoring. Scorings were visually corrected based on spot-check inspection. Data analyses and statistics were performed using the MATLAB software package (MathWorks), using the methods of [60] and [61]. Differences were tested post hoc by parametric statistical tests. Where necessary, p values were Bonferroni-corrected. The suggested 4 groups of results were classified by visual inspection. The following parameters were applied: a channel was categorized as generally UP or Down when more than 2/3 of all frequencies over 24h showed an increase or decrease of more than 1x log2 fold change. A channel as categorized as circadian when a spectral band was changed differently in the first 12h than in the second 12h. A channel was categorized as frequency band specific when over 24h the change of the frequency band was constant. A channel was categorized as vigilance state dependent when the changes in relative spectral power correlated with the underlying hypnogram. Several channels fulfill more than one criterion, the grouping is only intended to help visualization of the data.

Multi unit and LFP recordings

For multiunit activity (MUA) mice were recorded repeatedly for 2h starting at ZT1. The raw signal was sampled with 32kHz, highpass filtered at 500Hz, amplified and digitized using Multichannel Systems. The LFP signal was down sampled to 100Hz and bandpass filtered between 0.5-40Hz and. Spikes were detected based on voltage threshold (+/− 4 SD of the mean) and sorted based on PCA and sorted using the valley seeking method using the Plexon offline sorter. Units with low signal-to-noise ratio (< 10:1) were excluded. The researchers were blind to the experimental condition during the spike sorting.

AAV vector design

The AAVs used in the screen were all produced in-house employing BL2 safety procedures and a custom-designed vector. First, we cloned the RFP (Red Fluorescent Protein) and the RNAi hairpin-MIR30 insertion site from the pTRIPZ vector (GE Healthcare) into the

pAAV-CAG backbone (gift from D.Boison, Neurology, Legacy Health, Portland). The pTRIPZ was cut with AgeI/MluI and the resulting 1.1kbp fragment was ligated into the blunted pAAV-CAG (EcoRV/ XhoI). In this vector, the hairpin insertion sites are between EcoRI and XhoI and flanked by MIR30 sequences. We called this new AAV backbone pAAV-CAG-tRFP-shRNA in the subsequent text. For the design of RNAi hairpins, we followed guidelines from The RNAi Consortium (Broad Institute of MIT and Harvard). We cloned 2 hairpins per gene of interest in two separate plasmids. All hairpin sequences used are listed in Table S1. The AAVs used for local ADK manipulation (Gift from D. Boison) are described in [20].

AAV Production

AAVs were produced according to protocols from Cell Biolabs. All AAVs used in the screen were serotype 2 AAVs. Briefly, pAAV-CAG-tRFP-shRNA was co-transfected with pDG (gift from C. Fraefel, Virology Department, University of Zurich) into HEK cells and harvested 48-72h later. The AAV particle was purified and concentrated with the kit from CellBiolabs (VPK140) and stored in PBS at −80°C in 10ul aliquots. Functional titer was established in HEK cells. Briefly, HEK cells were infected with 10ul of concentrated virus in a 96-well plate; the virus was spun down onto the cells and left in the supernatant for 90min. 24h later, RFP expression levels of each infection was measured by fluorescence detection in an ELISA plate reader.

To test the knockdown efficiency, shRNA plasmids were co-transfected with a CMVluc-target plasmid in NB2 (Neuroblastoma2 (ATCC number: CCL-131) [62],). Remaining luciferase activity was assessed after 48h. The CMVluc-target plasmid contained 500 to 800bp of suspected target region (Table S2).

The viral spread *in vivo* was assessed post mortem by visual inspection. On average, the spread was between 0.5 and 1um^3, with its center in cortical layer IV.

RNA extraction and transcriptome analysis

Brains for transcriptomics were harvested four hours after light onset (ZT4) under baseline conditions and after sleep deprivation (N = 4, per condition). The tissue was immediately snap-frozen for later processing. RNA extraction was done with the RNAeasy Mini kit from QIAGEN with subsequent DNaseI treatment. Deep-sequencing and transcriptomic analysis (Gene Enrichment Data S1, raw data Data S2) was done at the Functional Genomic Center Zurich (FGCZ). The raw reads were first cleaned by removing adaptor sequences and trimming low quality ends. Sequence alignment of the resulting high-quality reads to the Mouse reference genome (build mm10) and quantification of gene level expression was carried out using RSEM (Version 1.2.19). The R software package from Bioconductor, edgeR (Version 3.8.2), was used to assess the statistical significance of differences in gene expression. Genes showing altered expression with adjusted p value < 0.05 (Benjamini and Hochberg method) were considered as differentially expressed. RUVseq (Remove Unwanted Variation in RNA seq Data) data analysis was carried out as described in [59], k value was set at 3. Datasets have been deposited in GEO (GEO: GSE132075 and GSE130276).

Immunofluorescence

Animals were perfused with ACSF according to the procedure of [63] at ZT4 under baseline conditions and after sleep deprivation. Coronal sections (50um diameter) were stained for GABA-A α1 receptor subunits (polyclonal, raised in Guinea Pig, gift of J.M Fritschy, 1:20'000) or SynGAP1 (Thermo Fisher, PA1-046, polyclonal) and imaged using a Zeiss LSM700 confocal microscope at 40x magnification, the exposure time and intensity was kept identical for both genotypes. Quantification of GABA or SynGAP1-containing puncta was conducted using the ImageJ platform and homemade routines [64], briefly, wild-type littermates were used to establish a threshold level for fluorescence intensity and speckle size. For each animal the whole picture frame was counted blinded, puncta at the edges were excluded.

QUANTIFICATION AND STATISTICAL ANALYSIS

If not indicated differently in the STAR Methods, the BioStats Package from MATLAB (R2018b) was used for all statistical analysis. Statistical details, such as statistical test, as well as precise n, p and F values for each experiment can be found in the figure legends. If not indicated differently, mean and standard error of the mean (sem) are used.

DATA AND CODE AVAILABILITY

The data generated in this study are available at GEO (transcriptomics, GEO: GSE132075 and GSE130276) or Zenodo (EEG recordings as MATLAB files and supplementary figure depicting raw spectral data, https://doi.org/10.5281/zenodo.2653232). All MATLAB code generated for this study is available upon request from the lead contact (Steven A. Brown, steven.brown@pharma.uzh.ch).